Analysis of black carbon on filters by image-based reflectance

Matthew Jeronimo[a,*], **Quinn Stewart**[a], **Andrew T. Weakley**[b], **Jason Giacomo**[b], **Xiaolu Zhang**[b], **Nicole Hyslop**[b], **Ann M. Dillner**[b], **Matthew Shupler**[a], **Michael Brauer**[a]

[a]School of Population and Public Health, University of British Columbia, Vancouver, British Columbia, V6T1Z3, Canada

[b]Air Quality Research Center, University of California – Davis, Davis, California 95616, United States

Abstract

Black carbon (BC) is an important contributor to global particulate matter emissions. BC is associated with adverse health effects, and an important short-lived climate pollutant. Here, we describe a low cost method of analysis that utilizes images of PTFE filters taken with a digital camera to estimate BC content on filters. This method is compared with two existing optical methods for analyzing BC (Smokestain Reflectance and Hybrid Integrating Plate and Sphere System) as well as the standard chemical analysis method for determining elemental carbon (Thermal-Optical Reflectance). In comparisons of aerosol generated under controlled conditions (using an inverted diffusion flame burner to cover a range of mass loading and reflectance levels) (N=12) and in field samples collected from residential solid fuel combustion in China and India (N=50), the image-based method was found to correlate well (normalized RMSE <10% for all comparisons) with existing methods. A correlational analysis of field samples between the optical methods and Fourier-transform infrared spectroscopy indicated that the same functional groups were predominantly responsible for light attenuation in each optical method. This method offers reduced equipment cost, rapid analysis time, and is available at no cost, which may facilitate more measurement of BC where $PM_{2.5}$ mass concentrations are already measured, especially in low income countries or other sampling efforts with limited resources.

Keywords

Black carbon; particulate matter; optical methods; reflectance measurement; rapid analysis

---

*Corresponding Author. Matty.Jeronimo@ubc.ca., Phone number: 604 822 9580.

Supporting Information

One supporting information Word document attached, including description and figure of black carbon generation apparatus and figures and discussion regarding interpretation of FTIR analysis.

Declaration of interests

The authors declare that they have no known competing financial interests or personal relationships that could have appeared to influence the work reported in this paper.

1. Introduction

Black carbon (BC) refers to the light-absorbing component of airborne carbonaceous aerosol. Black carbon is a common product of incomplete combustion and an important contributor to particulate matter (PM) emissions globally. In particular, emissions from residential combustion of solid fuels (e.g. coal, wood), biomass (open) burning and diesel combustion are major PM sources, where BC is a major constituent (Tami C. Bond et al. 2007). BC is itself associated with adverse health effects, including lung cancer and cardiopulmonary diseases, as well as an important short-lived climate pollutant, contributing to global warming (Attfield et al. 2012; Dockery et al. 1993; United Nations Environment Protection and World Meterological Organization 2011; Koch 2005; T. C. Bond et al. 2013; Santisi 2012; Chameides et al. 1999). In many cases Black Carbon offers more robust estimates of health effects than those for $PM_{2.5}$ mass concentrations (Janssen et al. 2011). Further, within urban areas Black Carbon demonstrates more spatial variability than $PM_{2.5}$ mass and is often considered as an indicator of traffic-derived particulate matter (Larson, Henderson, and Brauer 2009; Eeftens et al. 2012; Jedynska et al. 2014). Given its health and climate impacts, measurements of BC are especially useful for evaluating potential co-benefits, for example from reduction of emissions sources with high intake fractions such as residential combustion of solid fuels (Anenberg et al. 2012; Grieshop, Marshall, and Kandlikar 2011; Aung et al. 2016).

The term BC implies that solely optical methods are used for quantification. These methods rely on the relationship between the amount of BC on the surface of a sampled medium and the reflectance of light or transmittance of light through that medium. Optical methods include continuous instruments like Aethalometers (Sharma 2002; Drinovec et al. 2015) as well as techniques to measure reflectance or transmittance directly on sampled filters (Davy et al. 2017). Aethalometers have the advantage of monitoring continuously but can be expensive to purchase and maintain. The Laser Transmission Method (a version of the earlier Integrating Plate Method (Taha et al. 2007)) measures BC collected on a filter by comparing the transmission of a He-Ne laser at 633 nm through a loaded filter relative to that of a blank filter, thus allowing for the calculation of the absorption coefficient (Rosen et al. 1978; Lin, Baker, and Charlson 1973; Sadler et al. 1981). This method was further refined by addition of an integrating sphere and multiple detectors for simultaneous analysis of the transmitted and reflected signal, referred to as the Hybrid Integrating Plate and Sphere system (HIPS) (Campbell, Copeland, and Cahill 1995; White et al. 2016). The simultaneous determination of transmittance and reflectance reduces error due to variation in filter media and particle backscattering. The HIPS system has been used extensively and validated against co-located EC samples through the IMPROVE visibility and aerosol monitoring network (Malm et al. 1994). However, HIPS analysis also requires specialized equipment. Additional multi-wavelength methods based on integrating spheres and UV-VIS spectrometers have been used for refining BC measurements while also providing data on other colored components including brown carbon sources or heavy loadings of iron oxides (Lawless 2004; Yan et al. 2011). These methods are gravimetrically calibrated, rapid and non-destructive. However, initial equipment costs are a few thousand dollars and require in house modifications.

Smoke stain reflectance (SSR) has long been an inexpensive and accessible alternative optical BC measurement approach used frequently in exposure assessment and epidemiologic analyses (Cyrys et al. 2003; Janssen et al. 2011). SSR uses a white tungsten light and a photosensitive selenium cell to determine the percentage of light reflected by a filter (in reference to the value of a blank filter) which can then be related to the transmittance of the BC layer and thus the BC content of the filter (ISO/TC 146 1993). SSR is cheaper than other methods, but is susceptible to user error (stray light in room, prone to baseline drift, potential cross-contamination between filters [device touches filter]), time-consuming (around 1.5 hours for 10 samples) and assumes light absorption at any wavelength is due to BC, which cannot be assumed with environmental field samples.

These and other optical measurements of BC may be contrasted against measurement of elemental carbon (EC) by operationally-defined thermal methods.. Both the optical (i.e. BC) and thermal (i.e. EC) properties of aerosols are important but require different measurement methods. These methods require special instrumentation, samples must be collected on specially prepared quartz filters, and the filter is destroyed in the analysis. Furthermore, minor changes in temperature conditions used and/or samples enriched in inorganic content of the particulate matter (e.g. dust or metal) can dramatically change the fraction of a sample determined to be OC or EC by this method (Fung, Chow, and Watson 2002; Wang et al. 2012; Watson, Chow, and Chen 2005).

To extend BC analysis to settings with limited resources, including rapid analysis in field settings, Ramanathan et al. introduced the idea of employing cost-effective BC monitoring using a digital photograph of a sampled filter on a template and compared this approach to measurement of EC by thermal-optical analysis and BC by an aethalometer (Ramanathan et al. 2011). Other groups have described similar optical techniques to estimate BC directly from filters using colorimeters, scanners, and cameras (Khuzestani et al. 2017; Olson et al. 2016; Cheng, Chan, and Lau 2011; Du et al. 2011). These approaches may be especially useful in studies that lack the resources required for the more expensive quantitative techniques.

Paired with the increasingly common use of automated gravimetric filter analysis, the development of a semi-automated optical BC method would dramatically reduce time requirements of methods such as SSR. Recent advances in open-source image analysis and continued improvement in inexpensive image capture suggest the potential to extend the image-based approaches to an accessible, low-cost, and quantitative method. An image-based method may also be less susceptible to filter inhomogeneity and does not require any physical touching or handling of the filter. Accordingly, this paper describes a new semi-automated rapid image-based method of BC analysis and tests its viability as a non-destructive and cost-effective approach for BC analysis against the existing methods of SSR, EC by TOR, and HIPS (White et al. 2016). Fourier-transform infrared (FTIR) spectroscopy was used in a correlational study to ascertain the similarity of response to the chemical composition of the collected particles by each optical method.

2. Materials and Methods

2.1 Field Samples

Field samples were collected as part of the Prospective Urban and Rural Epidemiological (PURE) Air Household Air Pollution study at multiple sites in China and in Chennai, India (Arku et al. 2018). Briefly, personal and household (area) samples were collected at a flow rate of 1 L m^{-1} for 24 or 48 hours using the Ultrasonic Personal Aerosol Sampler (UPAS) from Access Sensor Technologies (Fort Collins, CO, USA) (Volckens et al. 2017). The filters used were barcoded 37mm PTFE filters, 2um pore size (PT37DMCAN-PF03, Measurement Technology Laboratories, Bloomington, MN, USA). Fifty field samples from the two field sites were selected to be analyzed by the image-based reflectance (IBR) technique and compared to SSR and HIPS. As real-world concentrations are typically log-normally distributed we did not randomly select filters but instead used mass concentrations and visual indication of darkness to select 50 filters spanning the distribution of absorbance levels. An additional ten field samples were repeatedly analyzed by SSR and IBR on five separate days to determine replicability. A paired household survey indicated the primary household cooking source of combustion for each filter, categorized as coal, gas, wood, agricultural residue/waste, or not identified.

2.2 Calibration Samples

Calibration samples consisting of varying amounts of pure elemental carbon deposited on filters were generated at the UBC Energy and Aerosols Laboratory using an inverted diffusion flame burner (Miniature Inverted Soot Generator, Argonaut Scientific, Edmonton, AB, Canada)(Kazemimanesh et al. 2019). Simultaneous duplicate samples were collected on PTFE filters (with no printed barcode) and quartz filters at 12 different loadings, visually estimated to span the range from high to low reflectance. The quartz filters were analyzed by Thermal/Optical Reflectance (Section 2.6) and the PTFE filters by Smoke Stain Reflectance (Section 2.3) Image-Based Reflectance (Section 2.4), and Hybrid Integrating Plate and Sphere (Section 2.5). The apparatus and collection methods are described fully in the supplementary materials.

2.3 Manual Smoke Stain Reflectance

The manual smoke stain reflectance (SSR) method utilized a Model 43 Reflectometer from Diffusion System Ltd. (London, UK) following the SOP established by the ESCAPE study(European Study of Cohorts for Air Pollution Effects (ESCAPE) 2002). The units used are percent reflectance and are defined by media blanks of the specific filters being used (defined as 100% reflectance) and a manufacturer-supplied calibration swatch (35% reflectance). The SOP specifies that to obtain a reflectance measurement for a filter, five measurement must be taken on each filter and averaged. However, as described in section 2.1, all the field sample filters had printed barcodes. Therefore, only three values could be obtained per filter, rather than the five specified in the SOP.

2.4 Image-Based Reflectance

The image-based reflectance (IBR) method utilizes an evenly-lit chamber in which the sample filter is placed, set onto an image template in a fixed position. A camera (Section 2.4.2) is set into the top of the chamber at a fixed distance from the filter and a picture is taken. This image of the filter and template can then be processed as described below to estimate the reflectance of the filter.

2.4.1 Chamber—The measurement chamber was constructed of cardboard and had dimensions of 31 cm wide, 31 cm long, and 21.5 cm high. The interior of the chamber was coated with the reflective side of aluminum foil. The chamber was illuminated by a grid of LED lights (5000K color temperature). The strips of LED lights were installed with double-sided tape in seven horizontal rows along the inside lid of the chamber as well as at the four vertical corners of the template from the top to halfway down. The template placed on the bottom of the chamber was 15.5 cm by 17.7 cm. A 6 cm by 6 cm square was cut in the middle of the measurement chamber lid for the lens of the camera. Individual filters in petri plate bottoms were placed in the middle of the circle on template inside the chamber. The neutral white LED lights lining the inner lid and four corners of the template chamber were turned on in order to evenly light the template and sample. A camera was mounted above the template chamber lid with a small opening for the lens to fit through.

2.4.2 Photo Acquisition

2.4.2.1 <u>Digital SLR:</u> The camera used was a Canon EOS Rebel T5i with a Canon EF-S 18–55MM f/3.5–5.6 IS STM lens. The camera was connected to a computer via a USB. The camera was positioned over the opening of the evenly lit chamber. A picture of the sample on the template was taken via tethered capture using Adobe Lightroom Classic CC version 7.3.1.

2.4.2.1.1 Effect of Chamber: To investigate the effect of the chamber itself on the absorbance data, the 50 field filters described in Section 2.1 were again photographed with the DSLR camera, but with no chamber. The 50 samples were photographed on the template which was placed on brown cardboard backing, under ambient lighting (overhead fluorescent lights).

2.4.2.2 <u>Cell phone:</u> As an alternative to the high-quality camera and template chamber described above, additional measurements were based upon photographs taken with two cellular phone cameras under ambient lighting. The 50 field filters described in Section 2.1 were photographed on the template which was placed on a brown cardboard backing. The filter was photographed with ambient lighting (overhead fluorescent lights) using an Apple iPhone 6s and a Moto G (3rd generation), taking care to not cast any shadows over the filter and template.

2.4.3 Creation of Calibration and Template—An initial calibration template was developed with ten boxes with known greyscale values from RGB = [0,0,0] to [255,255,255]. This template was printed on thick, matte texture paper. Each PTFE calibration filter was photographed on the calibration template. The mode of the red channel

(M_R) in the RGB color space was extracted for each of the ten greyscale boxes and for the filter surface. By interpolation, the theoretical M_R was determined for the filter – that is, the theoretical M_R a printed area would have to have to give the same M_R as the filter itself. This procedure allows for the design of a template (Figure 1) with 9 calibration squares that each represent a physical calibration filter with a known SSR value. An unknown PTFE filter can then be photographed on this template. A calibration curve can be constructed, with the M_R values of the calibration squares (extracted from the image each time) as the x-axis and their known SSR values as the y-axis. Then, given the M_R value of the unknown filter extracted from the image, the reflectance of the unknown filter R_S can be calculated.

2.4.4   Software Analysis—The actual acquisition of the image-based reflectance value was conducted using a custom Python script. The full code is available here (https://github.com/mjeronimo/reflectance). Briefly, the overall procedure was: using Open CV2 (Bradski 2000), the acquired sample image was compared to a stored image of the template and warped, cropped, and resized to a standard size and aspect, correcting for variations due to the angle or distance the photo was taken at. The 9 calibration squares were identified based upon their known position within the image and their M_R values extracted. With their reflectance values already known a calibration curve can be obtained. The user was then presented with an image of the filter and prompted to select the active area with a transparent circular cursor that defaults to the typical filter size and center of the image, but can easily be resized or moved. The M_R of the selected sample area was extracted and using a calibration curve built from the extracted M_R and known reflectance values for the 9 calibration squares a reflectance value R_S was calculated. Multiple filters can be analyzed in quick succession, with the selection of the active area and the calculation each taking only seconds.

2.4.5   Reflectance Data Analysis—For SSR and IBR, absorption or optical depth, τ (tau), was calculated according to the Beer-Lambert law:

$$T = e^{-\tau} = \frac{P}{P_0} \qquad\qquad \text{[Equation 1]}$$

Where T is transmittance, τ is optical depth, P_0 is incident radiation and P is transmitted radiation. We then calculated τ:

$$\tau = \ln\frac{P_0}{P} = 0.5\ln\frac{R_F}{R_S} \qquad\qquad \text{[Equation 2]}$$

Where R_F is the average reflectance of the field blank filters for a given batch of samples and R_S is the reflectance of the sample filter. The factor of 0.5 in Equation 2 is specified by ISO 9835:1993 to account for the assumption that the light reflected from the surface of the filter has passed through the layer of light absorbent particles twice.

For the purposes of this study, we have presented all absorbance results in terms of τ, which depends only on the filter analyzed and its loading. However, it is pertinent to specify that for atmospheric applications, the atmospheric absorption coefficient F_{abs} (units of Mm^{-1}) is calculated τ from and the known sample volume V and sample deposit area f:

$$F_{abs} = \frac{f}{V}\tau \qquad\qquad\qquad \text{[Equation 3]}$$

2.5 Hybrid Integrating Plate and Sphere System

Each sample's absorption optical depth (τ_{abs}) was measured from PTFE filters using a HIPS system at AQRC (White et al. 2016). Laser radiation (633nm) was directed at the unexposed side of the sample filter through an integrating sphere to capture the diffuse reflectance. Transmitted light was simultaneously collected using an integrating plate constructed of a neutral density filter and diffusing glass positioned behind the sample. The sphere and plate detectors were calibrated using 10 blanks prior to sample analysis.

2.5.1 HIPS Data Analysis—For the HIPS method (White et al. 2016), the absorption was calculated in terms of optical depth τ:

$$\tau = \ln\frac{P_0}{P} = \ln\frac{(1-r)}{t} \qquad\qquad\qquad \text{[Equation 4]}$$

Where r is the calibrated reflectance signal from the sphere and t is the calibrated transmittance signal from the plate.

2.6 Thermal/Optical Reflectance

Organic and elemental carbon (OC, EC) were determined from 18 quartz filters using the Sunset Laboratory OC/EC Aerosol Analyzer (Birch and Cary 1996)(Model 5L, Sunset Laboratory Inc.) with the IMPROVE_A thermal protocol and reflectance charring correction (Chow et al. 2007) at the Air Quality Research Center (AQRC) at the University of California, Davis . A punch of approximately 0.6 cm^2 in size was removed from each filter sample for TOR analysis. The sample punch was first heated (up to 580°C) in an inert (100% He) atmosphere where various OC fractions (OC1-OC4) volatilized. The system was then switched to an oxidizing atmosphere (90% He/10% O$_2$) where EC fractions (EC1-EC3) combusted at higher temperatures. A manganese dioxide (MnO$_2$) oxidizer was used to convert the liberated carbon compounds into CO$_2$, which was then reduced to CH$_4$ by a methanator and quantified by a flame ionization detector (FID).

During the thermal analysis, a fraction of the OC pyrolyzes or chars under the inert atmosphere into EC-like substances and can only be removed by combustion in the oxidation environment. The presence of the pyrolyzed OC (OP) can bias the estimation of EC high. To correct for this interference, the reflectance of the sample was continuously monitored throughout the analysis using a laser diode at a wavelength of 658 nm. The reflectance decreased in response to the formation of POC and then increased as the POC was combusted. The split between OC and EC is defined as the point in the oxidation stage when reflectance returned to its initial reading before the heating started. No correction on the dependency of laser reflectance on temperature was made during the post-processing. The reported OC and EC values are in areal density (µg cm^{-2} of a filter) and are not blank corrected.

2.7   Fourier-transform Infrared Spectroscopy

Fourier-transform infrared (FTIR) spectroscopy was used in a correlational study to ascertain which functional groups contribute to the instrument response of the SSR and IBR methods. Specifically, similar contributions of the same functional groups for each method would suggest similar underlying responses within each approach.

A correlational analysis using Fourier-Transform Infrared Spectroscopy (FTIR) was used to compare the relative sensitivity of each BC analysis method on a functional group level. Specifically, a given reflectance measurement was regressed onto concurrently-measured FTIR spectra using a partial least squares (PLS) calibration. Summary statistics derived from PLS components ascertain the relative importance of functional groups in better describing deviations in each method's aerosol optical depth; therefore, corroborating the similarity between methods.

2.7.1   Analysis—FTIR spectra were collected for each sample using the Bruker Tensor II using a liquid nitrogen cooled (77K) mercury cadmium telluride (MCT) detector. Following a five-minute purge of the instrument using compressed air scrubbed of carbon dioxide and water vapor, spectra were collected at $4cm^{-1}$ resolution. Transmission spectra were then ratioed against instrument background transmittance to remove any remaining water vapor and CO2 interference and converted to absorbance. A total of 50 spectra (n) were collected on PTFE filters with aerosols derived from coal, agricultural residue/waste, wood, gas and non-identified emission sources.

2.7.2   Correlational analysis using partial least squares—Smoke stain reflectance (SSR), imaged-based reflectance (IBR), and Hybrid Integrating Plate and Sphere System measurements were consecutively calibrated to FT-IR spectra using the multivariate partial least squares (PLS) method, facilitating a comparison between the two methods at a functional group level (Wold, Sjöström, and Eriksson 2001). Under any multivariate calibration scheme, each absorption measurement in the FT-IR spectra are treated as predictor variables, $[X] = (x_1, x_2, \ldots, x_p)$, and calibrated to a corresponding reflectance measurement (dependent variable, y) to develop a set of calibration factors (i.e., regression coefficients , b). Unlike FT-IR calibrations developed for the routine prediction of select aerosol species (Weakley, Takahama, and Dillner 2016), the infrared regions (wavenumbers) considered most important in "explaining" the relationship between the FT-IR spectra and reflectance measurements are explored using the variable importance in projection (VIP) metric to ascertain the relationship between functional group composition and aerosol optical depth (Chong and Jun 2005). Formally,

$$VIP_j = \sqrt{\frac{p \sum_{a=1}^{A} EV(\%)_{y,a} w_{aj}^2}{\sum_{a=1}^{A} EV(\%)_{y,a}}}$$

where VIP_j is the VIP score for the jth wavenumber, p are the number of wavenumber (predictors) used for calibration, $EV(\%)_{y,a}$ is the percentage of y-variance explained by the ath PLS component (a.k.a., latent variable), and w_{aj}^2 the squared normalized PLS loading

weights (Weakley, Takahama, and Dillner 2016). Since the PLS loading weights (w_{aj}) express the correlation between a PLS component and the reflectance measurement, a VIP score may be roughly interpreted as the explained-variance weighted average contribution of a given wavenumber to the correlation between FT-IR absorption and reflectance measurement. Therefore, plotting the VIP scores against wavenumber for the SSR and IBR calibrations provides qualitative insight into the deviation between the two reflectance methods at the functional group level.

3. Results and Discussion

3.1 Image-Based Reflectance Method vs. Smoke Stain Reflectance Method

Tabular data of all results is available in the related dataset(Jeronimo 2019). Calibration samples of known composition and field samples of unknown composition both correlated well between the image-based and smoke stain reflectance methods (Figure 2). The Root Mean Square Error (RMSE) for the calibration filters was 0.032 and for the field filters was 0.017; normalized RMSE $\left(\text{NRMSE:} \frac{RMSE}{\bar{y}}\right)$ was 4% for both. The relationship was linear up until the filter smoke stain reflectance approached 20% (indicated on the graph by a dashed line), the point beyond which the SSR method is not recommended to be used (Taha et al. 2007). Additionally, SSR and IBR were conducted repeatedly for a set of 10 field sample filters on five separate days, yielding precision (as calculated by the standard deviation of all analyses by a given method) below 0.5% for both methods.

Figure 3 compares the VIP scores for the SSR (black) and IBR (red) measurements calibrated to the same FT-IR spectra from 50 field samples. Notably, the SSR and IBR measurements are calibrated to FT-IR absorption to almost the exact same degree as indicated by very minimal deviations between their VIP scores across all wavenumbers. This demonstrates that in addition to their results being well correlated, the methods respond similarly at the functional group level. A full discussion of the FT-IR results including averaged FTIR spectra for each household source of combustion is included in the supplementary information.

One notable practical advantage of the IBR method is it does not require direct handling or touching of the surface of the sample filter. In SSR, the probe is placed directly on the surface of the filter, leading to the potential for cross-contamination and/or removal of particulate from the filter. Additionally, due to the fact that the IBR method uses the entire sampled surface of the filter, the IBR method is less sensitive to holes, uneven sample distribution, or other irregularities in the deposited sample layer. However, the IBR method may be sensitive to the flatness of the filter. In this study the filters used all laid perfectly flat, but PTFE filters from some manufacturers may have a curved surface. The effect of non-flat filters was not tested.

3.2 Image-Based Absorbance vs. Hybrid Integrating Plate and Sphere system Absorbance

The comparison between image-based absorbance results of the PTFE calibration filters versus the HIPS absorbance on the same filters is shown in Figure 4. With a linear

relationship and a NRMSE of 8% (for both calibration and field filters), the image-based method closely correlates to the HIPS method. The relationship between the image-based and HIPS absorbance data for the pure EC calibration filters was linear. In both Equations 2 and 4, the two methods are estimating the same parameter and thus should theoretically be equal. Thus, in Figure 4, the slope should theoretically be 1. In this case, while close to 1, the slope was 1.23, suggesting that the IBR method somewhat underestimates BC absorbance versus HIPS. This highlights the assumptions made in basing an absorbance calculation only on filter reflectance, most notably the assumption that reflected light in the SSR or IBR methods has been transmitted exactly twice through the filter. In the field samples the linear fit diverges at the highest absorbance samples (high filter loadings, low reflectance). A high degree of correlation between the two methods was not surprising, with both being optical methods analyzing similar regions of visible light (HIPS at one wavelength – 633 nm; IBR using the red channel of CMOS digital camera sensor data, corresponding to a sensitivity peak from approximately 550–680 nm, centered at 600 nm (Lesnichii, Petrov, and Cheremkhin 2013)). HIPS has the advantage of combining simultaneous transmittance and reflectance in one instrument, thus accounting for light scattered by the particulate matter components such as sulfate as well as correcting for variation in filter media. The VIP scores (Figure 3) for the HIPS method show a broadly similar profile to IBR and SSR, but with organic functional groups even more strongly correlated to absorption.

3.3 Image-Based Reflectance vs. Elemental Carbon by Thermal-Optical Reflectance

Figure 5 shows the image-based absorbance result of the PTFE calibration filters versus the EC content of the paired quartz calibration filters (determined by the IMPROVE_A TOR analysis, described in section 2.6). With a linear relationship and an RMSE of 0.7 μg cm^{-2} (NRMSE = 7%) the image-based method closely correlates to EC by TOR for the pure EC samples tested here. The comparison between SSR absorbance and EC by TOR is similar, with slightly higher R^2 and slightly higher RMSE of 1.1 μg cm^{-2} (NRMSE = 10%). Note the graph on the right reflects only 9 calibration filters, as two filters were damaged in the handling of the SSR procedure, illustrating one of the advantages of the IBR procedure (no direct contact with the filter surface). This relationship between image-based absorbance and EC by TOR illustrated here could be used to estimate EC content on sampled filters. Reflectance methods have been shown to be highly correlated to TOR EC analysis, for example in three European areas(Cyrys et al. 2003) and in an area impacted by woodsmoke (Noullett, Jackson, and Brauer 2006).However, no field sample comparison was possible for this analysis as the TOR method would require co-located duplicate field samples on quartz filters, which were not available in this study.

3.4 Comparison with cell phone cameras and effect of chamber

To confirm the assertion by Ramanathan et al. (Ramanathan et al. 2011) that an image of a filter taken with an ordinary cell phone camera without any special lighting is accurate enough to estimate BC, the same 50 field samples discussed in section 3.2 were analyzed by 3 additional variations on the image-based method. These conditions are described in section 2.4.2, but to summarize: same DSLR camera used as in section 3.2, but with no chamber; iPhone 6s camera, no chamber; and Moto G, no chamber. In Figure S4, these 3 methods plus

the original DSLR/chamber method are plotted against HIPS absorbance as a way to compare all 4 against the same data. Comparing S4a and S4b, it is apparent that a similar trend is seen with or without the chamber. However, the IBR data using the chamber has a much smaller NRMSE versus the HIPS data (8% NRMSE for DSLR with chamber, 20% for DSLR without chamber). The data from the cell phone pictures shows that for both cameras there is a strong correlation with the HIPS absorbance, but with higher NRMSE (28% for Moto G, 25% for iPhone 6s) and slopes that do not closely match each other or the DSLR. This data suggests that overall the exact slope of correlation between the IBR method and other optical methods is sensitive to the particular camera sensor being used. A cell phone and a copy of the template could be used in the field to estimate BC on filters immediately after sampling or in the lab as a low-infrastructure analysis method. However, using an image capture system with a DSLR tethered to a computer and an evenly-lit chamber will be more standardized (lighting is always the same, angle is always the same) and faster (automatic image capture and tagging of images) and which is an advantage when analyzing large numbers of field samples.

4. Conclusion

Black Carbon is a useful marker for combustion-derived particulate matter and has been linked to a range of adverse health impacts. In many cases Black Carbon offers more robust estimates of health effects than those for PM2.5 mass concentrations (Janssen et al. 2011). Further, within urban areas Black Carbon demonstrates more spatial variability than PM2.5 mass and is often considered as an indicator of traffic-derived particulate matter (Larson, Henderson, and Brauer 2009; Eeftens et al. 2012; Jedynska et al. 2014). In addition, Black Carbon is an important short-lived climate pollutant with impacts on radiative forcing via direct absorption and by altering albedo after deposition on reflective surfaces. Given its health and climate impacts, measurements of BC are especially useful for evaluating potential co-benefits, for example from reduction of emissions sources with high intake fractions such as residential combustion of solid fuels (Anenberg et al. 2012; Grieshop, Marshall, and Kandlikar 2011; Aung et al. 2016). Common methods for BC analysis typically use costly real-time instruments or destructive filter-based analyses, although the non-destructive smokestain reflectometer reflectance measurement is used frequently in exposure and epidemiologic studies. We developed a rapid, semi-automated non-destructive image-based reflectance (IBR) measurement amenable for processing large numbers of samples which improves greatly upon the cost, ease of use, and speed of obtaining reflectance data versus the smokestain reflectometer. This method also retains the same or better precision and expands the usable range (IBR is able to analyze filters with heavier loadings than SSR). Using a printed template onto which a filter is placed and its color compared against that of calibrated areas of the template through use of a camera and customized image-processing software, the new IBR method showed excellent agreement with both the SSR analysis and HIPS on PTFE filters and with EC as analyzed by TOR on quartz filters. As with SSR and HIPS, IBR is can be conducted on PTFE filters and is non-destructive, reducing the need for multiple filter samples (e.g. quartz and PTFE co-located samples) for determination of different components in PM and for preserving filters for additional analysis when desired. One technician may acquire reflectance data for 100 filters

Author Manuscript

in a single one hour session, with the required equipment being a camera, a barcode reader, and a computer. As there already exist fully automatic gravimetric analysis systems which include cameras, the IBR analysis may be fully automatable in the future. Additionally, the IBR method was tested with a consumer cell phone camera and found to function equally well to the DSLR camera initially employed. The reduced equipment cost, rapid analysis time, automated data processing, and free availability of the image template and processing code for the IBR method should facilitate more measurement of BC where PM2.5 mass concentrations are already measured, especially in developing countries or other sampling efforts with limited resources.

Supplementary Material

Refer to Web version on PubMed Central for supplementary material.

Acknowledgments

References

Anenberg Susan C., Schwartz Joel, Shindell Drew, Amann Markus, Faluvegi Greg, Klimont Zbigniew, Janssens-Maenhout Greet, et al. 2012 "Global Air Quality and Health Co-Benefits of Mitigating Near-Term Climate Change through Methane and Black Carbon Emission Controls." Environmental Health Perspectives 120 (6): 831–39. 10.1289/ehp.1104301. [PubMed: 22418651]

Arku Raphael E., Birch Aaron, Shupler Matthew, Yusuf Salim, Hystad Perry, and Brauer Michael. 2018 "Characterizing Exposure to Household Air Pollution within the Prospective Urban Rural Epidemiology (PURE) Study." Environment International 114 (May): 307–17. 10.1016/j.envint.2018.02.033. [PubMed: 29567495]

Attfield Michael D., Schleiff Patricia L., Lubin Jay H., Blair Aaron, Stewart Patricia A., Vermeulen Roel, Coble Joseph B., and Silverman Debra T.. 2012 "The Diesel Exhaust in Miners Study: A Cohort Mortality Study with Emphasis on Lung Cancer." Journal of the National Cancer Institute. 10.1093/jnci/djs035.

Aung Ther W., Jain Grishma, Sethuraman Karthik, Baumgartner Jill, Reynolds Conor, Grieshop Andrew P., Marshall Julian D., and Brauer Michael. 2016 "Health and Climate-Relevant Pollutant Concentrations from a Carbon-Finance Approved Cookstove Intervention in Rural India." Environmental Science & Technology 50 (13): 7228–38. 10.1021/acs.est.5b06208. [PubMed: 27253693]

Birch ME, and Cary RA. 1996 "Elemental Carbon-Based Method for Monitoring Occupational Exposures to Particulate Diesel Exhaust." Aerosol Science and Technology 25 (3): 221–41. 10.1080/02786829608965393.

Bond TC, Doherty SJ, Fahey DW, Forster PM, Berntsen T, DeAngelo BJ, Flanner MG, et al. 2013 "Bounding the Role of Black Carbon in the Climate System: A Scientific Assessment." Journal of Geophysical Research: Atmospheres 118 (11): 5380–5552. 10.1002/jgrd.50171.

Bond Tami C., Bhardwaj Ekta, Dong Rong, Jogani Rahil, Jung Soonkyu, Roden Christoph, Streets David G., and Trautmann Nina M.. 2007 "Historical Emissions of Black and Organic Carbon Aerosol from Energy-Related Combustion, 1850–2000." Global Biogeochemical Cycles 21 (2): n/a-n/a 10.1029/2006GB002840.

Bradski G 2000 "The OpenCV Library." Dr. Dobb's Journal of Software Tools. 10.1109/MRA.2009.933612.

Campbell Dave, Copeland Scott, and Cahill Thomas. 1995 "Measurement of Aerosol Absorption Coefficient from Teflon Filters Using Integrating Plate and Integrating Sphere Techniques." Aerosol Science and Technology 22 (3): 287–92. 10.1080/02786829408959747.

Chameides WL, Yu H, Liu SC, Bergin M, Zhou X, Mearns L, Wang G, et al. 1999 "Case Study of the Effects of Atmospheric Aerosols and Regional Haze on Agriculture: An Opportunity to Enhance Crop Yields in China through Emission Controls?" Proceedings of the National Academy of Sciences 96 (24): 13626–33. 10.1073/pnas.96.24.13626.

Cheng Jessica Y. W., Chan Chak K., and Lau Arthur P. S.. 2011 "Quantification of Airborne Elemental Carbon by Digital Imaging." Aerosol Science and Technology 45 (5): 581–86. 10.1080/02786826.2010.550960.

Chong Il-Gyo, and Jun Chi-Hyuck. 2005 "Performance of Some Variable Selection Methods When Multicollinearity Is Present." Chemometrics and Intelligent Laboratory Systems 78 (1–2): 103–12. 10.1016/j.chemolab.2004.12.011.

Chow Judith C., Watson John G., Antony Chen L-W, Oliver Chang MC, Robinson Norman F., Trimble Dana, and Kohl Steven. 2007 "The IMPROVE_A Temperature Protocol for Thermal/Optical Carbon Analysis: Maintaining Consistency with a Long-Term Database." Journal of the Air & Waste Management Association 57 (9): 1014–23. 10.3155/1047-3289.57.9.1014. [PubMed: 17912920]

Cyrys Josef, Heinrich Joachim, Hoek Gerard, Meliefste Kees, Lewné Marie, Gehring Ulrike, Bellander Tom, et al. 2003 "Comparison between Different Traffic-Related Particle Indicators: Elemental Carbon (EC), PM2.5 Mass, and Absorbance." Journal of Exposure Science & Environmental Epidemiology 13 (2): 134–43. 10.1038/sj.jea.7500262.

Davy Pamela M., Tremper Anja H., Nicolosi Eleonora M.G., Quincey Paul, and Fuller Gary W.. 2017 "Estimating Particulate Black Carbon Concentrations Using Two Offline Light Absorption Methods Applied to Four Types of Filter Media." Atmospheric Environment. 10.1016/j.atmosenv.2016.12.010.

Dockery Douglas W., Arden Pope C, Xu Xiping, Spengler John D., Ware James H., Fay Martha E., Ferris Benjamin G., and Speizer Frank E.. 1993 "An Association between Air Pollution and Mortality in Six U.S. Cities." New England Journal of Medicine 329 (24): 1753–59. 10.1056/NEJM199312093292401. [PubMed: 8179653]

Drinovec L, Mo nik G, Zotter P, Prévôt ASH, Ruckstuhl C, Coz E, Rupakheti M, et al. 2015 "The 'Dual-Spot' Aethalometer: An Improved Measurement of Aerosol Black Carbon with Real-Time Loading Compensation." Atmospheric Measurement Techniques. 10.5194/amt-8-1965-2015.

Du Ke, Wang Yang, Chen Bing, Wang Kai, Chen Jinsheng, and Zhang Fuwang. 2011 "Digital Photographic Method to Quantify Black Carbon in Ambient Aerosols." Atmospheric Environment 45 (39): 7113–20. 10.1016/j.atmosenv.2011.09.035.

Eeftens Marloes, Beelen Rob, de Hoogh Kees, Bellander Tom, Cesaroni Giulia, Cirach Marta, Declercq Christophe, et al. 2012 "Development of Land Use Regression Models for PM 2.5 , PM 2.5 Absorbance, PM 10 and PM Coarse in 20 European Study Areas; Results of the ESCAPE Project." Environmental Science & Technology 46 (20): 11195–205. 10.1021/es301948k. [PubMed: 22963366]

European Study of Cohorts for Air Pollution Effects (ESCAPE). 2002 "Determination of Absorption Coefficient Using Reflectometric Method" 2002 http://www.escapeproject.eu/manuals/ESCAPE-Reflection-sop.pdf.

Fung Kochy, Chow Judith C., and Watson John G.. 2002 "Evaluation of OC/EC Speciation by Thermal Manganese Dioxide Oxidation and the IMPROVE Method." Journal of the Air & Waste Management Association 52 (11): 1333–41. 10.1080/10473289.2002.10470867. [PubMed: 12469720]

Grieshop Andrew P., Marshall Julian D., and Kandlikar Milind. 2011 "Health and Climate Benefits of Cookstove Replacement Options." Energy Policy 39 (12): 7530–42. 10.1016/j.enpol.2011.03.024.

ISO/TC 146. 1993 "Ambient Air-Determination of a Black Smoke Index" Geneva, Switzerland: International Organization for Standardization.

Janssen Nicole A.H., Hoek Gerard, Simic-Lawson Milena, Fischer Paul, van Bree Leendert, Ten Brink Harry, Keuken Menno, et al. 2011 "Black Carbon as an Additional Indicator of the Adverse Health Effects of Airborne Particles Compared with Pm10 and Pm2.5." Environmental Health Perspectives. 10.1289/ehp.1003369.

Jedynska Aleksandra, Hoek Gerard, Wang Meng, Eeftens Marloes, Cyrys Josef, Keuken Menno, Ampe Christophe, et al. 2014 "Development of Land Use Regression Models for Elemental, Organic Carbon, PAH, and Hopanes/Steranes in 10 ESCAPE/TRANSPHORM European Study Areas." Environmental Science & Technology 48 (24): 14435–44. 10.1021/es502568z. [PubMed: 25317817]

Jeronimo Matthew. 2019 "Analysis of Black Carbon on Filters by Image-Based Reflectance - Filter Data." Mendeley Data. 10.17632/8krwmzjjrp.

Kazemimanesh Mohsen, Moallemi Alireza, Thomson Kevin, Smallwood Greg, Lobo Prem, and Olfert Jason S.. 2019 "A Novel Miniature Inverted-Flame Burner for the Generation of Soot Nanoparticles." Aerosol Science and Technology 53 (2): 184–95. 10.1080/02786826.2018.1556774.

Khuzestani Reza Bashiri, Schauer James J., Wei Yongjie, Zhang Yang, and Zhang Yuanxun. 2017 "A Non-Destructive Optical Color Space Sensing System to Quantify Elemental and Organic Carbon in Atmospheric Particulate Matter on Teflon and Quartz Filters." Atmospheric Environment 149 (January): 84–94. 10.1016/j.atmosenv.2016.11.002.

Koch Dorothy. 2005 "Distant Origins of Arctic Black Carbon: A Goddard Institute for Space Studies ModelE Experiment." Journal of Geophysical Research 110 (D4): D04204 10.1029/2004JD005296.

Larson Timothy, Henderson Sarah B., and Brauer Michael. 2009 "Mobile Monitoring of Particle Light Absorption Coefficient in an Urban Area as a Basis for Land Use Regression." Environmental Science and Technology. 10.1021/es803068e.

Lawless P 2004 "Multiwavelength Absorbance of Filter Deposits for Determination of Environmental Tobacco Smoke and Black Carbon." Atmospheric Environment 38 (21): 3373–83. 10.1016/j.atmosenv.2004.03.038.

Lesnichii VV, Petrov NV, and Cheremkhin PA. 2013 "A Technique of Measuring Spectral Characteristics of Detector Arrays in Amateur and Professional Photocameras and Their Application for Problems of Digital Holography." Optics and Spectroscopy 115 (4): 557–66. 10.1134/S0030400X13100093.

Lin Chin-I, Baker Marcia, and Charlson Robert J.. 1973 "Absorption Coefficient of Atmospheric Aerosol: A Method for Measurement." Applied Optics. 10.1364/ao.12.001356.

Malm WC, Sisler JF, Huffman D, Eldred RA, and Cahill TA. 1994 "Spatial and Seasonal Trends in Particle Concentration and Optical Extinction in the United States." Journal of Geophysical Research. 10.1029/93JD02916.

Noullett Melanie, Jackson Peter L., and Brauer Michael. 2006 "Winter Measurements of Children's Personal Exposure and Ambient Fine Particle Mass, Sulphate and Light Absorbing Components in a Northern Community." Atmospheric Environment 40 (11): 1971–90. 10.1016/j.atmosenv.2005.11.038.

Olson Michael R., Graham Eric, Hamad Samera, Uchupalanun Pajean, Ramanathan Nithya, and Schauer James J.. 2016 "Quantification of Elemental and Organic Carbon in Atmospheric Particulate Matter Using Color Space Sensing—Hue, Saturation, and Value (HSV) Coordinates." Science of The Total Environment 548–549 (April): 252–59. 10.1016/j.scitotenv.2016.01.032.

Ramanathan N, Lukac M, Ahmed T, Kar A, Praveen PS, Honles T, Leong I, Rehman IH, Schauer JJ, and Ramanathan V. 2011 "A Cellphone Based System for Large-Scale Monitoring of Black Carbon." Atmospheric Environment 45 (26): 4481–87. 10.1016/j.atmosenv.2011.05.030.

Rosen H, Hansen ADA, Gundel L, and Novakov T. 1978 "Identification of the Optically Absorbing Component in Urban Aerosols." Applied Optics. 10.1364/ao.17.003859.

Sadler M, Charlson RJ, Rosen H, and Novakov T. 1981 "An Intercomparison of the Integrating Plate and the Laser Transmission Methods for Determination of Aerosol Absorption Coefficients." Atmospheric Environment (1967) 15 (7): 1265–68. 10.1016/0004-6981(81)90318-8.

Santisi Jennifer. 2012 "Black Carbon's Big Impacts." E. Environ. Mag 23 (1): 13–15.

Sharma S 2002 "Light Absorption and Thermal Measurements of Black Carbon in Different Regions of Canada." Journal of Geophysical Research 107 (D24): 4771 10.1029/2002JD002496.

Taha Ghassan, Box Gail P., Cohen David D., and Stelcer Ed. 2007 "Black Carbon Measurement Using Laser Integrating Plate Method." Aerosol Science and Technology 41 (3): 266–76. 10.1080/02786820601156224.

United Nations Environment Protection, and World Meterological Organization. 2011 "Integrated Assessment of Black Carbon and Tropospheric Ozone. Summary for Decision Makers." Environment

Volckens J, Quinn C, Leith D, Mehaffy J, Henry CS, and Miller-Lionberg D. 2017 "Development and Evaluation of an Ultrasonic Personal Aerosol Sampler." Indoor Air 27 (2): 409–16. 10.1111/ina.12318. [PubMed: 27354176]

Wang Mo, Xu Baiqing, Zhao Huabiao, Cao Junji, Joswiak Daniel, Wu Guangjian, and Lin Shubiao. 2012 "The Influence of Dust on Quantitative Measurements of Black Carbon in Ice and Snow When Using a Thermal Optical Method." Aerosol Science and Technology 46 (1): 60–69. 10.1080/02786826.2011.605815.

Watson John G., Chow Judith C., and Antony Chen L-W. 2005 "Summary of Organic and Elemental Carbon/Black Carbon Analysis Methods and Intercomparisons." Aerosol and Air Quality Research 5 (1): 65–102. 10.4209/aaqr.2005.06.0006.

Weakley Andrew T., Takahama Satoshi, and Dillner Ann M.. 2016 "Ambient Aerosol Composition by Infrared Spectroscopy and Partial Least-Squares in the Chemical Speciation Network: Organic Carbon with Functional Group Identification." Aerosol Science and Technology 50 (10): 1096–1114. 10.1080/02786826.2016.1217389.

White Warren H., Trzepla Krystyna, Hyslop Nicole P., and Schichtel Bret A.. 2016 "A Critical Review of Filter Transmittance Measurements for Aerosol Light Absorption, and de Novo Calibration for a Decade of Monitoring on PTFE Membranes." Aerosol Science and Technology 50 (9): 984–1002. 10.1080/02786826.2016.1211615.

Wold Svante, Michael Sjöström, and Lennart Eriksson. 2001 "PLS-Regression: A Basic Tool of Chemometrics." Chemometrics and Intelligent Laboratory Systems 58 (2): 109–30. 10.1016/S0169-7439(01)00155-1.

Yan Beizhan, Kennedy Daniel, Miller Rachel L., Cowin James P., Jung Kyung-hwa, Perzanowski Matt, Balletta Marco, Perera Federica P., Kinney Patrick L., and Chillrud Steven N.. 2011 "Validating a Nondestructive Optical Method for Apportioning Colored Particulate Matter into Black Carbon and Additional Components." Atmospheric Environment 45 (39): 7478–86. 10.1016/j.atmosenv.2011.01.044. [PubMed: 22125411]

Highlights

- Current black carbon analysis techniques are expensive, destructive, or time-consuming.

- Image-based reflectance is a viable solution for on-site resource-limited sampling efforts which currently rely on outsourcing for data analysis.

- A DSLR or cellphone camera was used to assess black carbon on filters with results comparable to existing optical methods.
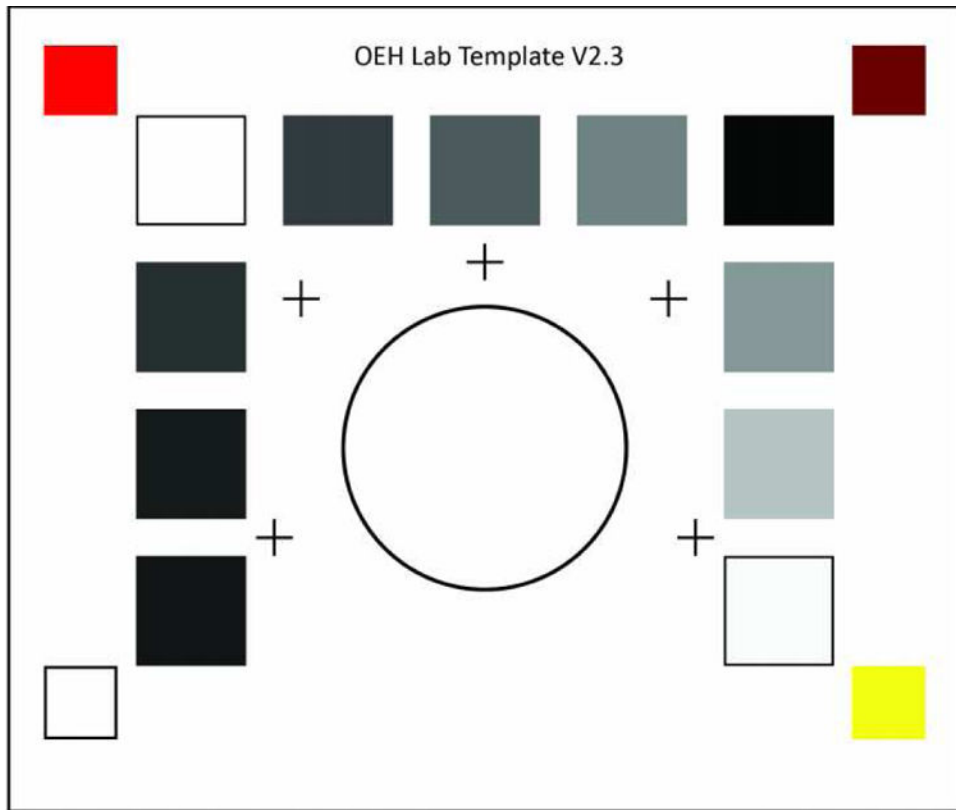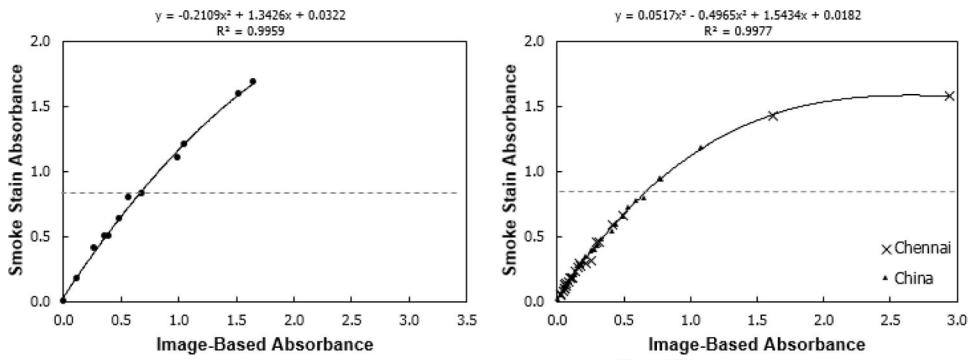
Figure 1 -
Final Template

$$y = -0.2109x^2 + 1.3426x + 0.0322$$
$$R^2 = 0.9959$$

$$y = 0.0517x^3 - 0.4965x^2 + 1.5434x + 0.0182$$
$$R^2 = 0.9977$$

Figure 2 -

Optical depth, tau, comparisons between the Image-Based Reflectance method and Smoke Stain Reflectance method for 12 calibration filters (left) and 50 field samples (right). Approximate smoke stain reflectance of 20% is indicated by the dashed line. SSR is not recommended to be used on filters with a reflectance of <20% (corresponding roughly to an optical depth τ of >0.8 (Taha et al. 2007).
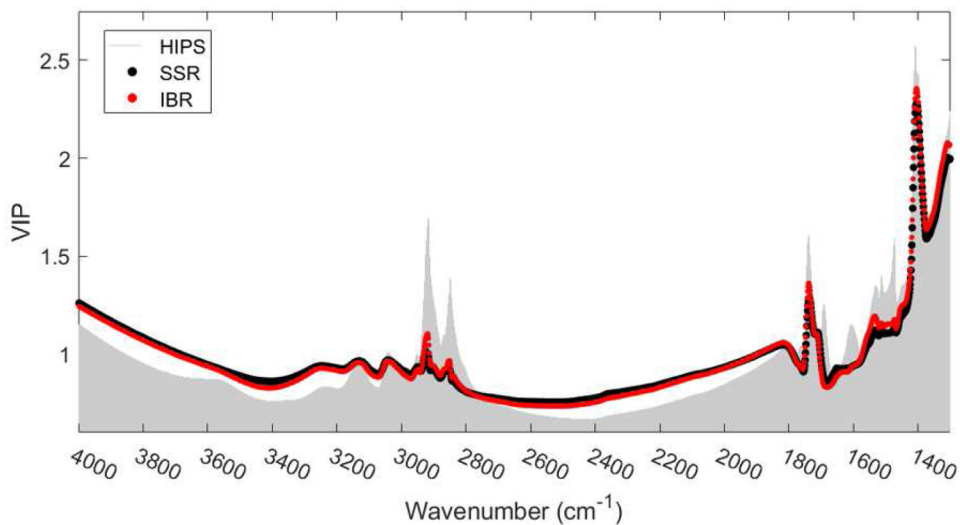
Figure 3 -

Variable importance in projection (VIP) scores illustrating wavenumbers most important when calibrating IBR, SSR, and HIPS measurements to the FT-IR spectra using the PLS algorithm. A good fit was observed between the SSR and IBR measurements and spectra according to the coefficient of determination (R^2) equal to 0.870 and 0.806, respectively. VIP scores greater than or "near" 1 are generally considered important in describing the relationship between the dependent and predictor variables (Chong and Jun 2005).
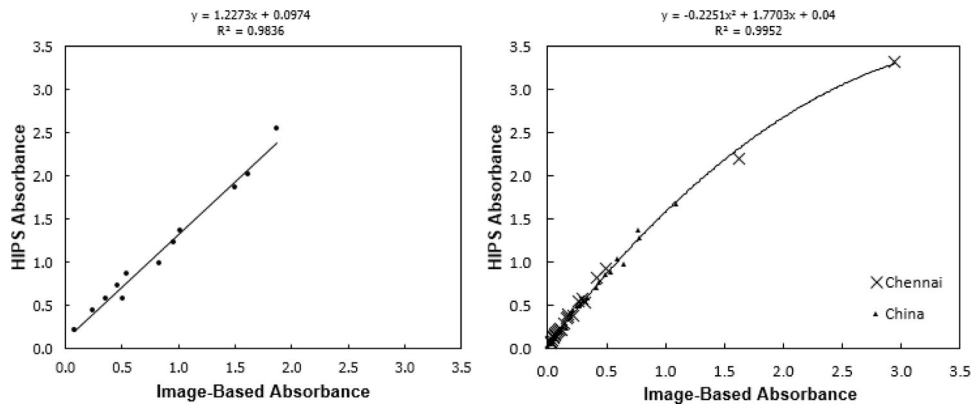
$$y = 1.2273x + 0.0974$$
$$R^2 = 0.9836$$

$$y = -0.2251x^2 + 1.7703x + 0.04$$
$$R^2 = 0.9952$$

Figure 4 -
Image-Based Absorbance vs. HIPS Absorbance on 12 calibration filters (left) and 50 field samples (right)
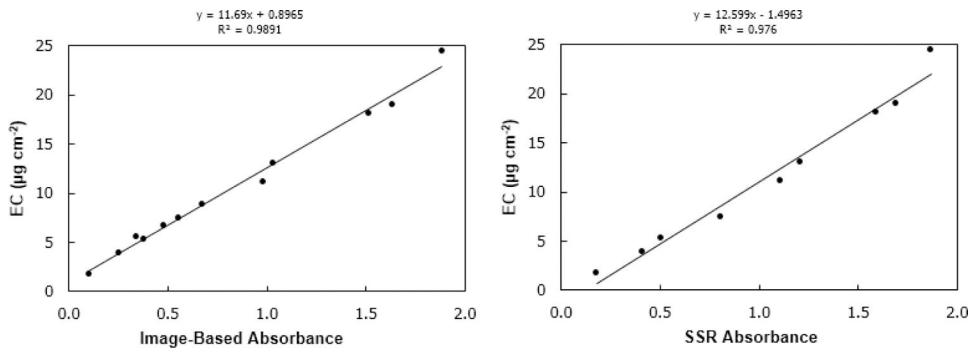
Figure 5 -

Image-based absorbance vs elemental carbon by thermal/optical reflectance, 11 calibration filters (left). SSR absorbance vs elemental carbon by thermal/optical reflectance, 9 calibration filters (right).